5 March 04
Ref No: 809

1st Ind to MNGG Memo, 9 Feb 04, Requests for Review and Clearance

AFRL/MN CA-N

MEMORANDUM FOR AAC/PA

I recommend that the attached paper titled "Emissive Infrared Projector Real-Time Scene Data Pixel Processing" be approved for public release.

ROBERT L. SIERAKOWSKI, ST
Chief Scientist
Munitions Directorate

18 March 2004

2nd Ind, AAC/PA

TO: AFRL/MN CA-N

Approved.

JIM I. SWINSON
Office of Public Affairs

AAC/PA 04-132

DEPARTMENT OF THE AIR FORCE
AIR FORCE RESEARCH LABORATORY (AFMC)
EGLIN AIR FORCE BASE, FLORIDA

11 MAR 2004

MEMORANDUM FOR AFRL/MN CA-N

FROM: AFRL/MNGG

SUBJECT: REQUEST FOR REVIEW AND CLEARANCE

1. Request review and approval of the attached paper for public release. Pertinent information is as follows:

a. TITLE OF PUBLICATION: Emissive Infrared Projector Real-Time Scene Data Pixel Processing

b. AUTHORS: Owen Williams, Leszek Swierkowski, August Huber, George C. Goldsmith II, James Norman, and Larry Herald

c. TITLE OF FORUM: Technologies for Synthetic Environments: Hardware-in-the-Loop Testing IX

d. SPONSOR: The International Society For Optical Engineering

e. LOCATION AND DATE (S): Orlando, FL; April 12-16, 2004

f. CLASSIFICATION OF CONFERENCE OR FORUM: Unclassified

g. CLASSIFICATION OF PAPER: Unclassified

h. FOREIGN NATIONALS WILL BE PRESENT

i. The paper will be published in the proceedings.

j. Deadline: 15 March 2004

k. JON: 10620101

2. The material contained in the attached paper is technically accurate, unclassified, and suitable for public release.

3. Even though key words that appear in the paper are included in the U.S. Munitions List (USML) (International Traffic in Arms Regulation (ITAR), 22 Code of Federal Regulations (CFR) Part 121), and/or Commerce Control List (CCL), (Export Administration Regulations (EAR) Part 774, Categories 0-9), the particular aspect of technology that the paper addresses is not included as part of the USML and/or the CCL,

#409

does not meet the definition of critical technology as defined by DoDD 5230.25, and will not result in the transfer of any military critical technology.

4. If you have any questions please contact Lt Rachel Moore AFRL/MNGG, 882-4446, EXT 2289.

SANDRA M. LEFSTAD, DR-IV
Chief, Advanced Guidance Division

Emissive infrared projector real-time scene data pixel processing

Owen M. Williams*[a], Leszek Świerkowski[a], August J. Huber[b],
James D. Norman,[c] George C. Goldsmith II[c], W. Larry Herald[d]

[a]Defence Science and Technology Organisation, PO Box 1500, Edinburgh, Australia 5111

[b]AEgis Technologies Group Inc., Huntsville AL

[c]Air Force Research Laboratory Munitions Directorate, Eglin AFB, FL 32542-6810

[d]MacAulay-Brown Inc., One 11th Ave, Suite B-4, Shalimar FL 32579

ABSTRACT

The new generation PC-based array control electronics (PACE) system for emissive infrared projector real-time scene data processing has opened the potential for the development of more complex real-time nonuniformity correction (RNUC) algorithms than were formerly possible. In this paper, emitter array response data are analyzed in order to identify the underlying physical processes and to identify the form of the RNUC algorithm they suggest. It is shown that although the PACE system is capable of processing the algorithm, the development of a practical RNUC processor would seem to be limited by the complexities that underlie the observed variability in emitter response.

Keywords: dynamic infrared scene projection, real-time processing, nonuniformity correction

1. INTRODUCTION

The need for real-time processing to overcome the inherently nonlinear response and nonuniformities associated with emissive infrared projector pixels has long been recognized. The nonlinear radiant response is determined by the combination of digital-to-analog converter (DAC) response, the nonlinear characteristics of the drive field-effect transistor (FET), the quadratic variation I^2R of the electrical power applied to the emitter resistance, the nonlinear response of the consequent emitter temperature rise and the strong Planck radiation law increase of in-band emitter radiance with increasing temperature. Because of nonuniformities associated with each of the underlying processes, the individual emitter responses vary in both magnitude and shape.

The real-time processing techniques that are almost universally applied today to offset both nonlinearity and nonuniformity evolved over a period of years, inspired by the needs of the Ballistic Missile Defense Office (BMDO) guided interceptor programs and from the work of Kinetic Kill Vehicle Hardware-in-the-Loop Simulator (KHILS) staff at USAF Research Laboratory. In 1994 Stockbridge *et al.*[1] reported on the nonlinear and nonuniform characteristics of the 128 × 128 Honeywell NODDS arrays available at the time and presented the first analysis on how the required nonuniformity correction (NUC) might be performed. In 1997, Jones *et al.*[2] reported on the sparse grid method of nonuniformity measurement applied to 512 × 512 Wideband Infrared Scene Projector (WISP) arrays and introduced a 'simplified' NUC procedure in which the concept of linearizing the emitter responses through use of a nominal average response curve was introduced. As they highlighted, the significance of this step was that it led towards the design of a tractable real-time nonuniformity correction (RNUC) method in which the demands applied to individual emitters could be corrected by a single gain and offset combined with a global lookup table (LUT) used for applying the necessary linearization transformation. In later work, Olson and Murrer[3] reported on the refinement of the linearization method

* *Email:* owen.williams@dsto.defence.gov.au; leszek.swierkowski@dsto.defence.gov.au; august.huber3@eglin.af.mil; james.norman2@eglin.af.mil; george.goldsmith@eglin.af.mil; herald@eglin.af.mil

through the introduction of multiple breakpoints, allowing piecewise linear fitting in the linearized domain designed to counter the effects of residual nonlinearities. Olson and Murrer also reported the first RNUC hardware implementation within the KHILS laboratory. Since that time, the same hardware and its antecedents have become established as providing the essential interface between the input real-time scene generator and the majority of the fielded Honeywell WISP, MSSP, BRITE 1 and BRITE 2 emitter arrays.

It is interesting that the linearization method in the advanced form reported recently by Sieglinger *et al.*[4] now incorporates curve-fitting, introduced to reduce measurement scatter and to increase the correlation between the successive gains and offsets that characterize the neighboring linearized curve segments. Curve-fitting lies at the heart of the alternative "physics-based" or "process-based" techniques that have been proposed. The first attempt at developing a physics-based NUC solution was made by Malone in the mid-1990s for the KHILS laboratory, as alluded to by Malone and Flynn,[5] but was abandoned in favor of the simpler and more easily realizable linearization method. More recently,[6,7] however, we have been exploring the curve-fitting alternatives and their potential for application without breakpoints over wider regions of the dynamic range. We continue that interest within this paper.

The most prominent driver is the availability of the new generation PC-based array control electronics (PACE) system[8] developed recently to replace the legacy RNUC hardware and to enable the interfacing of both Honeywell and Santa Barbara Infrared (SBIR) emitter arrays to PC-based real-time scene generators. Significant within the present context is that the PACE system enables the real-time operation of more complex RNUC algorithms than were previously possible. It is therefore appropriate to examine whether the algorithm that can be derived by following the processes that lead to radiant emission can be practically implemented within the PACE system. This defines the theme of this paper.

Our conclusion is ambivalent. On the positive side we have been able to show that the PACE system has the capability of processing the real-time algorithm that emerges from detailed analysis of our measured MSSP emitter response data. Furthermore, our analysis has led to an improved understanding of the physical processes involved in the transformation from drive volts through to projected in-band radiance. However, the complexity of those processes and the consequent variety in emitter response have forced the algorithm and the identification of the necessary NUC coefficients to be rather more complicated than might be considered desirable. It is therefore judged that incorporation of physical process information of the type identified here is the more likely future for application within RNUC algorithm development.

2. THE REAL-TIME SCENE DATA PROCESSING REQUIREMENT

The functional requirement of the real-time processor within an infrared projection system can be deduced from the general block diagram shown in Figure 1. Note that commanded and projected radiances are each specified in the in-band signal radiance form

$$\Delta L_s = \Delta L - \Delta L_b , \tag{1}$$

where ΔL and ΔL_b represent the total and background in-band radiances. In Figure 1, capitalized V represents the actual voltage output from the digital-to-analog converter (DAC) applied to the projection array while lower case v represents the digital word applied to the DAC. For simplicity, we shall assume that v lies in the normalized range [0,1] and that any DAC nonlinearities are corrected within the DAC system block. In particular, as is clear from Figure 1,

$$v = \frac{V - V_{\min}}{V_{\max} - V_{\min}} . \tag{2}$$

It is also necessary that the signal radiances be normalized. For NUC purposes, the signal radiance at the camera output needs to be normalized with respect to the signal radiance ΔL_s^{ref} recorded from a reference emitter driven by maximum DAC volts; that is, by $v = 1$. Usually the maximum radiance recorded from the least acceptable performer is selected, by examining the histogram of all emitter responses at maximum drive volts and applying a suitable operability

criterion;[3] *e.g.*, that 99.9% of emitters generate more radiance than the least acceptable performer. Normalized radiances are denoted in lower case form Δl_s.

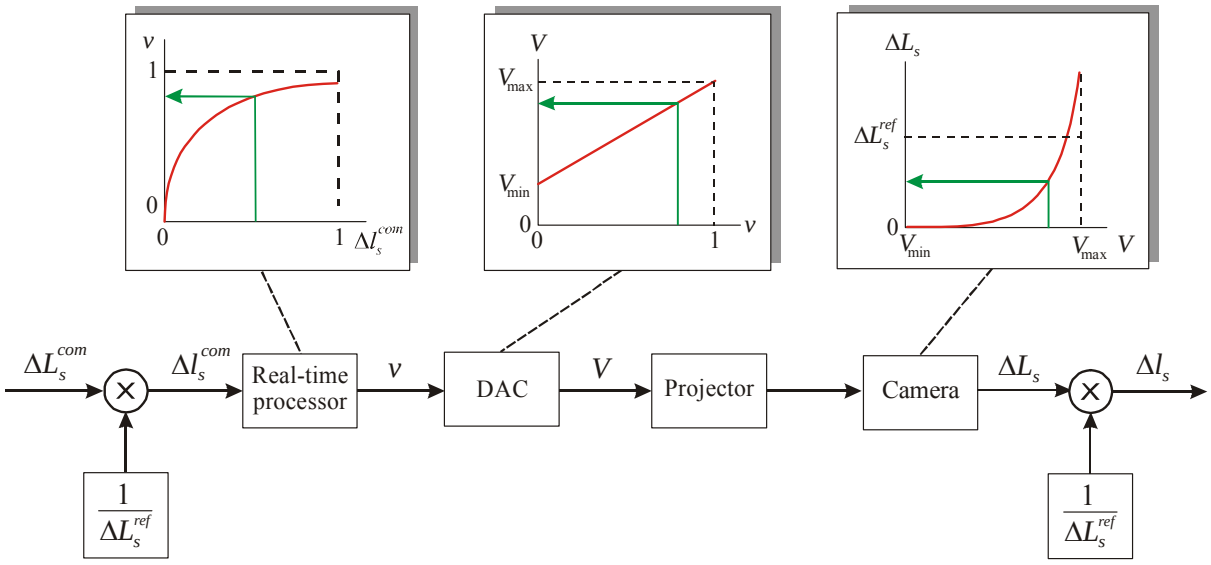

Figure 1: Projector scene data transfer (with half maximum radiance command highlighted)

By referring to Figure 1, it can be seen that the action of the processor on the command word Δl_s^{com} can be written in general functional form

$$v = g\left(\Delta l_s^{com}\right) \tag{3}$$

while the projected radiance can be similarly written as

$$\Delta l_s = f\left(v\right) = f\left[g\left(\Delta l_s^{com}\right)\right]. \tag{4}$$

Clearly, since we wish to match Δl_s to Δl_s^{com}, the objective for each emitter is to select the processor transfer function g that most closely matches the emitter inverse transfer function f^{-1}. It is this that defines the goal of both the linearization and curve-fitting techniques.

In fact, curve-fitting and linearization are merely different approaches to the same problem. One way to derive g for each emitter is to curve-fit the measured f^{-1}. In the alternative linearization method, g is initially represented by a global transfer function selected by averaging over a subset of the normalized emitter responses and then inverting; that is, g is initially chosen as a normalized global approximation to f^{-1}. When array response data are recorded with g loaded in the real-time processor, the resulting output Δl_s is approximately linear with the command radiance Δl_s^{com}, consistent with the reciprocal actions of f and g within (4). Indeed, in an ideal system where the emitter responses differ only by a gain factor, Δl_s will then be exactly proportional to Δl_s^{com}.

Practically, however, no single global transformation is capable of exactly replicating across the range of the differing inverse emitter responses. It is therefore necessary to apply piecewise linear corrections prior to the linearization procedure in order to successively improve the match between Δl_s and Δl_s^{com}. According to eqn (4), the net result is the generation of an emitter-specific inverse response function g. This is the same as the function that would have been generated by curve-fitting the inverse response function. Within this perspective, then, linearization and curve-fitting can be viewed as one and the same.

3. FIRST GENERATION RNUC PROCESSING

The legacy VME system on which the first generation of RNUC processors was based follows variants of a design that originally consisted of four 9U × 400 mm VME boards: a scene input board, an RNUC board, an array personality board and a RAMIX commercial-off-the-shelf (COTS) memory board. Image data from either RS-170, SGI or the RAMIX memory was formatted within the scene input board, the stored gains and offsets were applied in the RNUC board by using the breakpoint method while a global look-up table (LUT) within the personality board provided the linearization transformation.

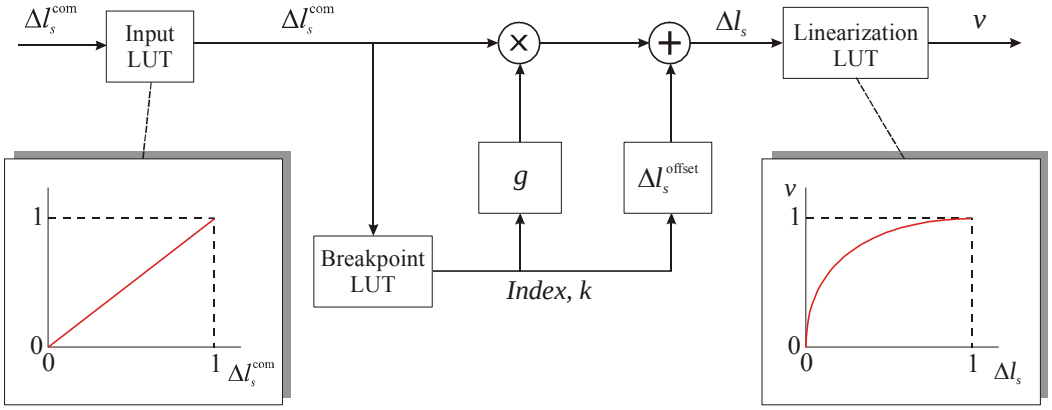

Figure 2: Legacy RNUC processor block diagram

In order to explore the potential for the development of advanced RNUC procedures we first consider the linearization method that was developed and implemented within the legacy KHILS laboratory RNUC hardware and which is still applied successfully today. A block diagram showing the available real-time processing functions is shown in Figure 2. Note that the input global LUT available on the scene input board is not used traditionally. Instead it is bypassed or filled in passthrough mode to replicate the command word, as is illustrated in Figure 2.

By following the nonuniformity measurement procedure described in earlier papers,[3,7] the dynamic range covered by the radiance command word is divided into a number of segments separated by breakpoints. The segments are determined by an index k output from the breakpoint LUT, while the emitter- and segment-specific gain and offset values that follow are stored in random access memory locations on the RNUC board. In following the simple algebra seen diagrammatically in Figure 2, we see that the input command word ΔI_s^{com} is converted into the segment-specific form

$$\Delta I_s\left(px,k\right)=g\left(px,k\right)\Delta I_s^{com}\left(px\right)+\Delta I_s^{offset}\left(px,k\right). \tag{5}$$

The actual values of the gain and offset coefficients and their constraints are not discussed here. Of greater interest is the fact that the input dynamic range has been divided by the breakpoints into a number of piecewise linear segments. In effect, the proportional transfer function that characterizes the input passthrough LUT has been transformed by the breakpoint processor into a continuous piecewise linear function. When this input is applied to the global LUT the net transform is piecewise-curved, continuous in value at the breakpoints but discontinuous in slope.

Application of the linearization technique has been highly successful.[4] The temperature resolution at low signal levels can, however, be limited. This has been addressed earlier.[9] The limitation is most acute for the medium-wave infrared (MWIR) band where the signal radiance between 0.1ºC and 400ºC differs by more than five orders of magnitude. Given the current standard of 16 bits of resolution over a 400ºC dynamic range, the lowest bit can be shown[9] to equate to 0.4ºC; that is, the desirable goal of 0.1ºC resolution within the low signal thermal imaging region is unattainable.

This problem can been overcome by providing 18 bits of effective resolution, as can be effected with little error[9] by appropriately combining the red, green and blue 12 bit output channels from the DDO2 port of a Silicon Graphics Inc. (SGI) Onyx series computer image generator, followed by a nonlinear global LUT within which a 18-bit to 16-bit down-conversion is effected. For example, if a radiance-to-temperature transformation is chosen for the latter the 0.1ºC to 400ºC dynamic range is reduced to 4000, easily covered by 16 bits of resolution. The 18-bit combination method has been implemented within the DSTO Primary Infrared Projection (PIRSP) system developed for DSTO Australia.[10]

In spite of the resolution problem being overcome through application of the radiance-to-temperature transformation, curve-fitting errors between the breakpoints still exist. The new PACE system, however, appears to offer the potential for implementing a curve-fitting algorithm without breakpoints over wider regions of the dynamic range. We therefore turn to examine the type of RNUC algorithm that needs to be explored to exploit this potential.

4. INVERSE EMITTER RESPONSE CURVE-FITTING

4.1 Array response data and calibration

In order to design any RNUC algorithm that extends in capability across much of the dynamic range, it is necessary to have available a data set that covers the complete range of emitter responses. In our previous paper[7] we reported the use of such a data set, recorded by applying the sparse grid method using the KHILS laboratory infrared projector development station with a Honeywell MSSP 512 × 512 snapshot array chosen as the test article. The measurement process and the preliminary processing required to assemble a complete set of array maps covering the 1.6-3.2V drive voltage range have been described earlier.[7]

The analytical steps are worthwhile repeating since they are relevant to the curve-fitting algorithm design of interest here. Signal radiance is calculated as

$$\Delta L_s^{BB}(\Delta T) = \Delta L^{BB}(T) - \Delta L^{BB}(T_b), \tag{6}$$

where T and T_b here represent the emitter and background apparent blackbody temperatures respectively and where

$$\Delta T = T - T_b \tag{7}$$

is the temperature difference. The respective in-band blackbody radiances were calculated by integrating the blackbody spectral radiance over the camera spectral responsivity $R(\lambda)$, the latter being normalized to unity at its peak wavelength; that is, for each T

$$\Delta L^{BB}(T) = \int_{\Delta\lambda} \frac{R(\lambda)}{R(\lambda_p)} \frac{c_1 / \lambda^5}{\exp\left(\frac{c_2}{\lambda T}\right) - 1} \, d\lambda \tag{8}$$

where c_1 and c_2 are the Planck equation radiation constants found in any standard blackbody radiation text. With this information, the camera counts above background were easily converted into signal radiance by comparing the radiances calculated at the calibration points with the corresponding measured counts.[7]

4.2 Generation of physical temperature estimates

In seeking a curve-fit solution it is desirable to attempt to understand the physical processes that underlie the observed emission characteristics. Unraveling the effects of the various processes is not an easy matter, however, since little information is available apart from the emitter responses themselves. Nevertheless, it remains an objective to separate out the processes where possible. It is from subsequent modeling that the mix of global functions and emitter-specific coefficients that constitutes the RNUC algorithm architecture can be derived.

The first step is to give consideration to the emitter emissivity and its nonuniformity. In our previous paper[7] we attempted unsuccessfully to explain the apparent 'bloom' on the array maps in terms of a low spatial frequency emissivity nonuniformity. The fact that our test failed does not mean that emissivity nonuniformities do not exist; rather, that we have not been successful in separating them out. Indeed, in Section 4.4 below we introduce some circumstantial evidence that may point to the existence of emissivity nonuniformity. Nevertheless, in the absence of specific information, the only possible way to proceed is to adopt the opposite extreme; that is, to assume a global emissivity value within the emitter attenuation coefficient[11-13] g_a. Here, g_a is the product of the in-band emissivity, emitter effective fill factor and transmission coefficient of the ZnSe vacuum isolation window in front of the array. After the subsequently-applied radiance-to-temperature transformation any emissivity nonuniformity that exists will effectively be mixed with the other sources of nonuniformity.

If $\Delta L_s(\Delta T)$ is the recorded signal radiance at physical temperature difference ΔT above background, the signal radiance $\Delta L_s^{BB}(\Delta T)$ that would have been recorded had the emitter been a blackbody (*i.e.*, if $g_a = 1$) equals $\Delta L_s(\Delta T)/g_a$. In the case of the MSSP array, values of 70% emissivity, 50% effective fill factor and 90% window transmission have been assumed, leading to the estimate $g_a \sim 0.3$. By inverting eqn (6) with appropriate use of the Planck equation (8), ΔT can then be extracted as the best estimate of the physical temperature of the emitter above background. Examples of the derived temperature responses are shown in Figure 3.

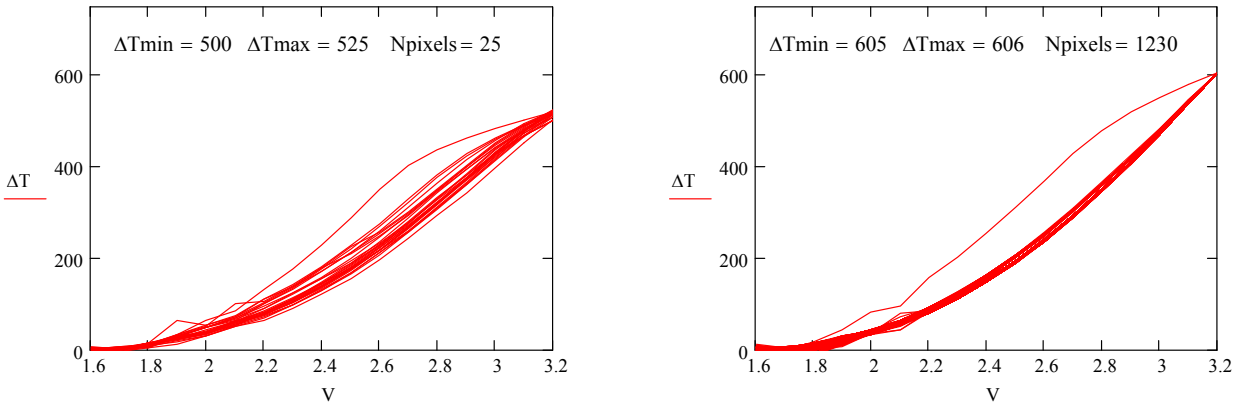

Figure 3: Selected temperature responses and 3.2V temperature histogram

As discussed earlier,[7] the vast majority of the temperature responses appear to vary approximately parabolically with drive voltage, except towards the higher drive levels where some exhibit downward curvature. This latter effect is most pronounced for the poorer performers, with a few exceptions as exemplified in Figure 3 by the single oddly-shaped emitter response. Such responses are discussed below in Section 4.4.

4.3 Estimated current/voltage characteristics

It is desirable to delve further by extracting the emitter current response to drive voltage. This step can be accomplished from the power balance relationship that exists since the delivered electrical power I^2R is dissipated almost exclusively as thermal power conducted down the emitter legs. Radiative power is negligible at all but the highest emitter temperatures, as can readily be estimated. Given this power balance, the current delivered to the emitter from the drive MOSFET can be calculated as

$$I = \sqrt{\frac{G\,\Delta T'}{R}} = \sqrt{\frac{G\left(\Delta T - \Delta T_0\right)}{R}} \tag{9}$$

where both the thermal conductance G and the emitter resistance R are temperature-dependent quantities and where we have introduced an emitter-dependent offset ΔT_0 to insure that the adjusted temperature difference ΔT' never falls below

zero. Although not evident from Figure 3, the derived temperature differences ΔT are observed to asymptotically approach both positive and negative values.[7] This is not unexpected since within the derivation of ΔT it has been tacitly assumed that the subtracted background temperature is global in nature. The data indicate otherwise. Clearly, however, the current I must fall to zero below the MOSFET threshold voltage and cannot be imaginary. Unfortunately, the low drive data was of insufficient quality to allow the ΔT_0 values to be extracted by extrapolation of the ΔT data to low drive levels. For simplicity at this exploratory stage, therefore, all negative values were merely set to zero. The relevance of the temperature correction is discussed below within Section 5, in relation to the RNUC algorithm design.

Temperature-dependent trends for both thermal conductance and resistance have been published earlier by Cole et al.[14] who showed that the thermal conductance rises with temperature and the resistance falls. Both of these trends lead to slower rises in temperature with drive current than would be expected if G and R were both temperature-independent, as can be seen by inverting eqn (9). Santa Barbara Infrared (SBIR) Inc. have graciously assisted with the present analysis by supplying their most recent $G(T)$ and $R(T)$ information for MSSP-like array materials. Examples of the temperature responses and current/voltage characteristics derived through use of this information are shown in Figure 4. Note that the units of I are the same as SQRT(ΔT) since only relative values of G and R were applied within the analysis.

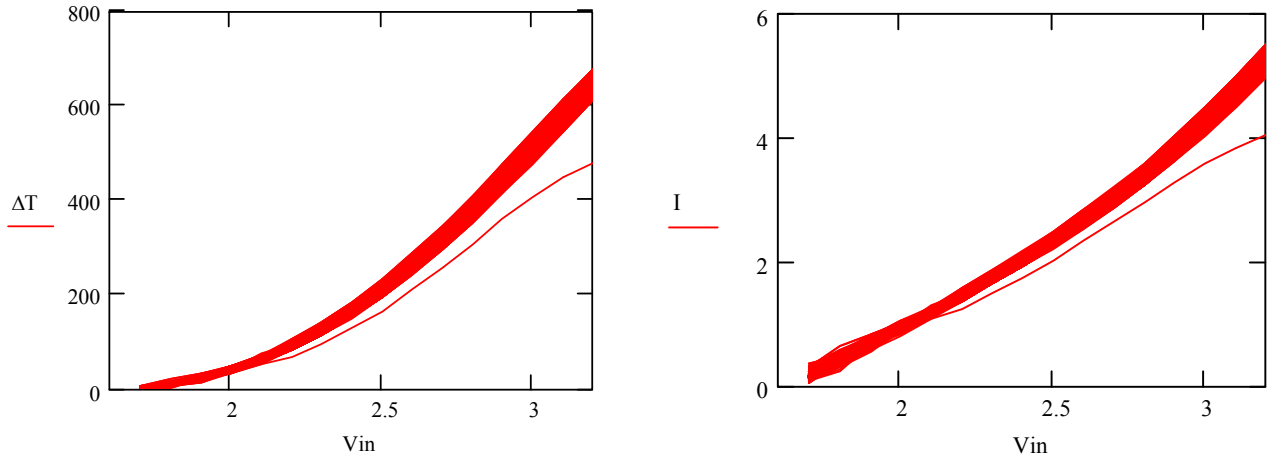

Figure 4: Temperature responses and derived current/voltage characteristics (column#2, MSSP array)

There are a number of interesting observations that can be made. Firstly, although not highly significant, the trend towards downward curvature at high drive levels has been largely removed, except for the single oddly-shaped response. We are therefore able to attribute the most common source of downward temperature response curvature to the high temperature increase in leg thermal conductance and fall in emitter resistance. Of greater significance, however, is the fact that at the lower drive levels the derived I-V responses exhibit significantly smaller curvature than do the corresponding temperature responses. This is largely a result of the action of the SQRT function within (9). As seen from Figure 4, the significance is that we can now extrapolate with some confidence to determine the individual MOSFET threshold voltages, a step that is not readily possible from the corresponding temperature responses (and even less so from the source radiance data).

At the lower drive levels we find that the I-V characteristics can be well-fitted to a quadratic form. This is consistent with the expected characteristics of the Honeywell emitter array MOSFETS.[6,14,15] Deviations from a quadratic fit assumption applied to the I-V characteristics seen in Figure 4 are shown in Figure 5 where the fitting procedure has been confined to the 1.7-2.5V drive range. Above this range the I-V characteristics clearly do not follow a simple quadratic form, a result that is not unexpected since there have been a number of tacit assumptions within the model that have thus far been applied. Most notably, emissivity nonuniformity has been folded into the temperature and current domains when it properly should be corrected within the radiance domain. Emissivity has also tacitly been assumed to be temperature-independent and further, the conductance and resistance temperature dependencies supplied

by SBIR Inc. have been assumed to be accurate for the MSSP array under test. MOSFET saturation also is not taken into account.

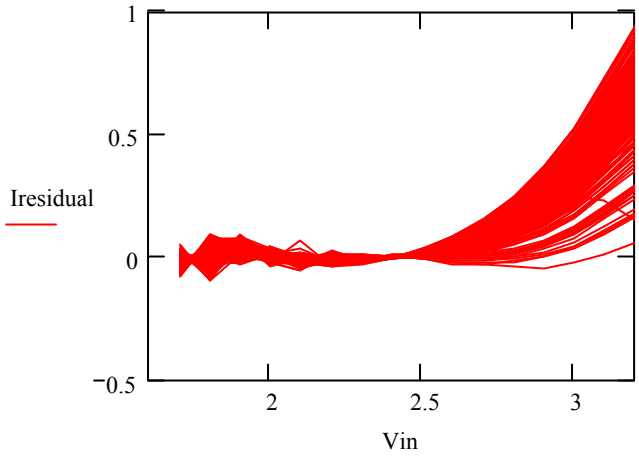

Figure 5: Residual current after quadratic fit

It is clear that the process model developed this far is not capable of describing the full range of physical processes. Nevertheless, it does show some promise at the lower drive levels relevant to thermal imager simulation. If we use the quadratic fit to define the core I-V dependence we can adjust it at the higher drive levels by adding the measured deviations from quadratic behavior. Indeed, by applying the threshold voltage quadratic expression adopted in an earlier paper,[6] we can express the current in the form

$$I = B\left(V - V_{th}\right)\left(V - V_{th} - \Delta V_{th}\right) + I_{\text{residual}}\left(I\right). \tag{10}$$

This equation can be solved analytically to generate the required drive voltage V; *viz.*,

$$V = V_{th} - 0.5\,\Delta V_{th} + \sqrt{0.25\Delta V_{th}^2 + \frac{I - I_{\text{residual}}\left(I\right)}{B}} = V'_{th} + \sqrt{C + \frac{I - I_{\text{residual}}\left(I\right)}{B}}. \tag{11}$$

The significance of this result is that it can be calculated in real-time within the PACE system, as discussed in Section 5 below. However, before that, it is worthwhile examining some of the potential advantages that might be available through use of such a form:

- Over the lower part of the dynamic range up to physical temperature differences of the order of 200ºC (130ºC calculated MWIR apparent temperature difference for the MSSP array used in this study[11-13]), eqn (11) can be calculated without the need for significant residual current correction, as can be seen by examining Figures 4 and 5. There is therefore potentially no need for breakpoints over this range.
- The MOSFET threshold voltage nonuniformity parameters have been separated from the emitter-specific nonuniformity parameter B. Without digressing into detail, it can be stated that B is similar to the form defined in an earlier paper[6] and therefore incorporates the nonuniformities associated with the emitter resistance, a MOSFET current scaling parameter and the thermal conductance. Of these, the emitter resistance is regarded as the most important since it is this that is likely to change with use as the emitters age. The advantage, therefore, is that the aging parameters have been grouped into a single nonuniformity coefficient. This could be significant in the future in relation to the potential for the development of a simplified daily NUC procedure based on the updating of only a single nonuniformity coefficient.

The residual current correction is most simply applied by using piecewise-linear fitting within a standard breakpoint architecture. In order to derive the required gain and offset coefficients the emitter response data needs to be prepared in the form shown in Figure 6, within which the positions of the breakpoints need to be specified. Note the example of

the poor performer and its limited response to the current demand. While the residual current for this emitter could be accommodated within the breakpoint architecture it is more likely that the example shown in Figure 6 would be rejected as an example of an unacceptable performer; that is, its response most likely would be specified as being inferior to that of the specified least acceptable performer and therefore rejected. Nevertheless, some good performers (*e.g.*, as seen in Figure 3 right) display the same type of oddly-shaped response and still need to be accommodated.

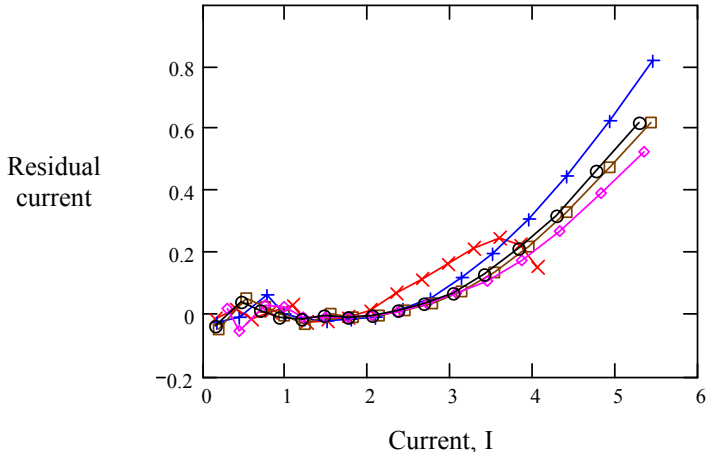

Figure 6: Examples of residual current variation with current demand

4.4 Evidence for emissivity nonuniformity

Before we proceed to discuss the practical implementation of the desired RNUC algorithm, it is worthwhile digressing briefly to speculate on the reason for the existence of the oddly-shaped emitter responses seen in Figures 3 and 4 above. According to power balance equation (9) the rise in physical temperature is simply I^2R/G. Within this relationship, neither the FET nonuniformities nor those associated with the leg thermal conductance are expected to cause such grossly different responses as that exemplified by the single emitter seen in Figure 3 right. The fact that this emitter is capable of achieving such high physical temperatures indicates that its resistance must be high. This does not, however, explain its oddly-shaped response.

Suppose, however, that this emitter is also characterized by low emissivity and that therefore, because of its poor radiative efficiency, it is actually being heated to much higher physical temperatures than those indicated in Figure 3. Since these higher temperatures are accompanied by even higher thermal conductances and lower emitter resistances than those associated with normal emitters, it is expected that the downward curvature that is observed would be pronounced. Note further that the downward trend could also be caused (or at least supplemented) by falling emissivity with increasing temperature.

An argument based on the combination of low emissivity and high resistance at first sight seems to be asking for somewhat of a coincidence. However, suppose that the raw emitter resistance before annealing was sufficiently high that the odd emitters became overheated during the anneal process, to the point where their structure was damaged and emissivity severely reduced. Low emissivity then becomes a direct consequence of high resistance and the need to rely on coincidence is removed.

We believe that the above argument, although admittedly speculative, is plausible. The fact that resistance is suspected as being the key physical property leading to the generation of oddly-shaped responses is consistent with both its known wide variability before anneal and its known changes during the anneal process.[14] As such, tighter control of resistance during the array manufacturing processes is seen to be highly desirable. Whether or not this will be possible to achieve is a matter for the array manufacturers.

Whatever the cause of the oddly-shaped responses, their existence is somewhat of a nuisance. Indeed, their presence undoubtedly complicates the development of the advanced RNUC algorithms being sought in this and other studies, the subject to which we now turn.

5. SECOND GENERATION (PACE SYSTEM) RNUC PROCESSING

The fundamental theme within this paper has been to explore the potential of process-based RNUC algorithms in improving post-NUC array uniformity, given the potential of more complex RNUC algorithms being implemented within the new PC-based array control electronics (PACE) system[8] and the concurrent steady move towards PC-based real-time scene generators.[16-18] The basic PACE system consists of the Timing and Input Processor (TIP) board, the Reconfigurable Pixel Processor (RPP) board, and an output board, all of which reside in a control PC. The addition of an SBIR array output interface board is required to drive the latest generation of SBIR arrays. These boards are PCI-based designs utilizing the control computer PCI bus, not only to load register and memory contents on the board, but also to reconfigure the firmware in the FPGAs. Information is passed between the boards over a simple Low-Voltage Differential Signaling (LVDS) interface. The current PACE system can support 512 × 512 arrays at frame rates up to 800 Hz and 1024 × 1024 arrays at frame rates slightly over 200 Hz.

One of the potential processing sequences required for real-time implementation of the RNUC algorithm explored above is shown in Figure 7. It is assumed that the PC scene generator can support 32-bit floating-point processing throughout its graphics pipeline and that the DVI word output into the red, green and blue channels of the frame buffer can be coded as a 24-bit word. In his 2003 AeroSense conference presentation,[16] Olson showed that the latter step can be effected simply through use of a single OpenGL fragment command.

5.1 Initial processing

The availability of floating-point graphics programming and the 24-bit word transfer from the scene generator to the PACE system displaces the need for the RGB recombination method[9] discussed earlier. The requirement for a minimum of 18 bits dynamic range to cover the full extent of a 0.1-400ºC MWIR infrared radiance requirement, however, still remains. We have discussed several options for inputting the 24-bit word output through the DVI port of the scene generator into the PACE system and have decided that the best approach that optimizes the use of the PACE resources is to strip the unused top 6 bits.

The subsequent processing step reveals a dilemma. If we follow the mathematical processing steps outlined in the above sections, illustrated here in Figure 7, we find that in the initial processing steps we need to provide the combination of an initial nonlinear LUT for effecting the required 18- to 16-bit global down-conversion from radiance to temperature, an emitter-specific subtraction for the background temperature offset correction ΔT_0 and a second 16-bit LUT in which the global transformation (9) from temperature to current is effected. The advantages of this approach are that the potential exists for additional processing, if necessary, within the intermediate temperature domain (for example, application of voltage overdrive[19] for risetime improvement) and that the ΔT_0 correction can be effected at 16 bits. The disadvantage is that two LUTs are required rather than a single combined radiance-to-current LUT. If the latter approach were adopted the ΔT_0 correction would instead need to be implemented as an equivalent radiance correction applied at the 18-bit input word level.

Regardless of which implementation is pursued, the initial LUT will be located on the TIP board. If the down-conversion/radiance-to-temperature transformation is accomplished in the first LUT the scene information is passed between the TIP and RPP boards in the same way as for the breakpoint method currently implemented on the PACE system. If, however, the scene information needs to be processed at 18-bit format before down-conversion and subsequent 16-bit RNUC processing a system throughput penalty exists since the throughput rate between the boards will then be halved. Since the PACE system can process scene data at high rates, however, this only limits the frame rate for a scene to 400 Hz. The resulting operation is therefore still twice as fast as any currently available 512 × 512 emitter array technology.

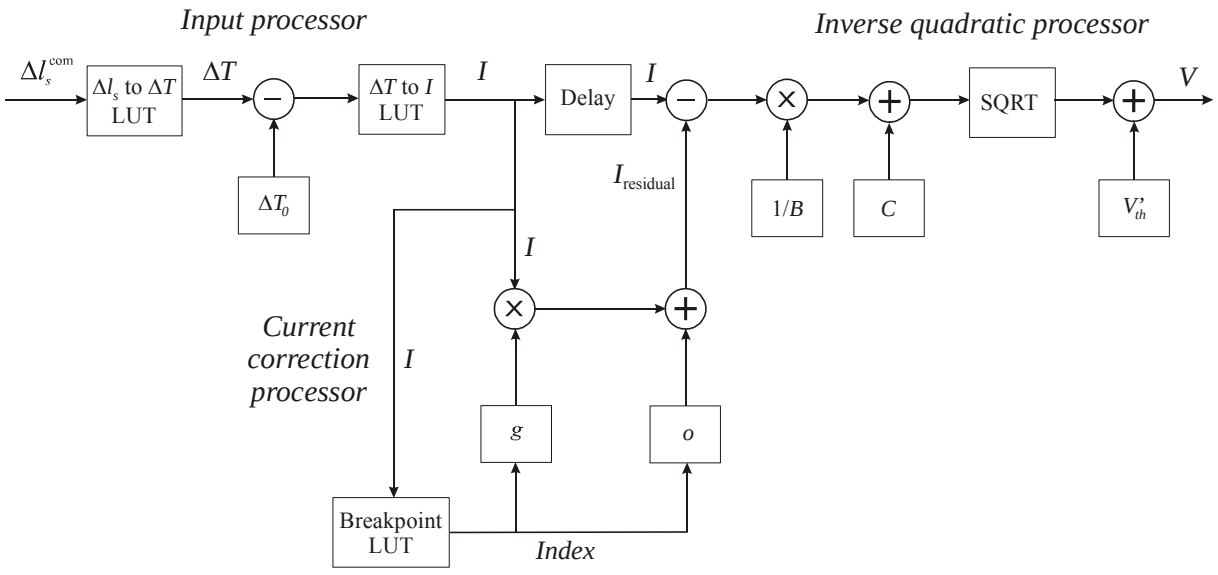

Figure 7: RNUC algorithm

Otherwise, processing in 18-bit format versus 16 bit-format has no significant impact on the logic resources used in the FPGAs. In fact, the dedicated multiplier circuitry incorporated in the FPGAs is based on an 18 × 18 multiplier and are therefore under-utilized at the 16-bit level. In both approaches, therefore, the offset correction and associated underflow protection are easily accommodated in the RPP board.

5.2 Background temperature correction

A second dilemma exists, this time unresolved. As has been discussed earlier, the ΔT_0 adjustment required to correct what seems to be local variations in the apparent background radiance can be either positive or negative. The question arises as to whether these variations are real or are merely artifacts arising from the array data measurements; for example, from camera drift or residual camera nonuniformity. If real, the variations could be caused by aliasing associated with the combination of the emitter sub-structure and the non-unity mapping used during the sparse grid measurement procedure, or from variations caused by background reflections. If on the other hand the variations are merely artifacts of the measurement procedure, the question arises as to whether a correction term such as ΔT_0 should be applied or not.

In the case that the observed effect is real, a correction term must be applied. In effect, this enables a flat pseudo-background level to be achieved at a certain low value of command voltage level. Below that level the output after the ΔT_0 correction will be negative for those emitters that display high apparent background radiances. If operation at such low levels is required it will be necessary either to set the output to zero or to remove the sign bit prior to the subsequent processing [which incorporates the square root within the temperature to current transformation (9)]. Whatever the choice, however, array outputs below that corresponding to the pseudo-background level will be invalid.

The above questions are interesting in the sense that they have never before come to the fore. The reason is one of the objectives underlying the present study: to search for alternative RNUC algorithms that potentially extend the dynamic range to low signal regions beyond the reach of the linearization technique within its current implementation. What is clear from the above discussion and the dilemma that has been posed is that further high quality measurement data at low drive levels and better knowledge of the NUC camera operational characteristics will be necessary precursors before the questions that have been posed can be satisfactorily answered. In future work we hope to return to this topic.

5.3 Residual current and inverse quadratic processing

Downstream of the input processors, it is suggested in Figure 7 that the residual current correction required before implementation of the inverse quadratic equation (11) be effected through the use of a standard breakpoint processor. The number of breakpoints and their positioning would need to be decided on the basis of analyzed residual current information, such as that illustrated in Figure 6. The breakpoint processor can easily be accommodated within the PACE system. Note that a delay needs to be introduced in the direct path for the current I to insure that it is present on the correct clock cycle to allow the residual current output from the breakpoint processor to be subtracted. The delay would be implemented through use of a series of pipeline delay registers, the number equaling the number of pipeline steps within the breakpoint calculations; for example, if 48 clock cycles are required for the breakpoint multiply and offset (as is the case for the conventional breakpoint RNUC algorithm), I would need to be clocked through 48 registers.

Regarding implementation of the inverse quadratic equation (11), it is recommended that a prior 16-bit to floating-point word transformation be effected in order to offset potential problems associated with integer data overflows and underflows and to offset the need for scaling to avoid the truncation and bit resolution problems inherent to integer data processing.[6] Conversion to and from floating-point format together with multiplication, addition and subtraction conforming to the IEEE-754 floating-point standard have previously been successfully implemented in firmware on the RPP board in support of spatial correction algorithms. For the Figure 7 RNUC application, the use of 32-bit floating point coefficients will be necessary together with the utilization of larger and faster FPGAs that are now available. Note that the legacy RNUC hardware cannot support floating-point calculations nor the use of 32-bit coefficients, and incorporates slow and bulky SRAM modules. In contrast, PACE can easily support the 32-bit coefficients loaded within on-board SDRAM. Indeed, one of the key challenges in implementing the conventional breakpoint RNUC algorithm within the initial PACE system was the development of firmware for the FPGAs on the RPP board to allow random access to the SDRAM modules at the rates required. With the development of this firmware, it can be stated that the RPP board has the resources and processing power to implement the floating-point breakpoint processor required here.

According to eqn (11), the breakpoint processor needs to be followed first by an emitter-specific gain $1/B$, then by an offset C, a SQRT function and a final threshold voltage offset term. The gain and offset coefficients will be stored in SDRAM and applied on the RPP board using floating-point precision. Although a pipelined floating-point SQRT function has not yet been implemented, appropriate firmware can currently be purchased from several vendors. Based on vendor literature, the SQRT function will require two to three times the resources required for a floating-point multiply. The subsequent threshold voltage offset can easily be implemented in floating-point and the result converted back to a 16-bit integer representation for input to the DAC.

As previously mentioned, KHILS has implemented a spatial correction algorithm on the RPP board using floating-point calculations. This application required 16 floating-point multiplies, 10 floating-point additions and conversions to and from floating point, all of which consumed 56% of the logic resources available on the FPGA. Since that time, technology has advanced to the point where the RPP board can now be populated with FPGAs of 33% larger size. Based on previous resource utilization and availability of the larger FPGAs performing the required two floating point multiplies, three floating point additions, the single SQRT function and conversion to and from floating point, the RNUC algorithm proposed here can easily be accommodated.

6. SUMMARY

In this paper we have explored the potential design of an advanced RNUC processor for improving the spatial fidelity of the dynamic scenes from emissive infrared projectors and for extending the region of the dynamic range over which the performance improvement can be effected. Our study has shown that the problem we are attempting to tackle is complicated by the variability within the physical processes taking place in the conversions from the input command word through to the output projected infrared radiance. Indeed, it is acknowledged that there is some doubt as to whether or not it is practical to base the design of the required advanced RNUC processor solely on knowledge of the underlying processes.

In spite of this doubt, the study has been useful in identifying a number of design areas that need to be addressed, regardless of the design philosophy that is ultimately chosen. Although it is difficult to predict at the present time we consider it most likely that the type of advanced processor to emerge from studies such as this and from the continuing development of practical infrared projector system knowledge, will be a hybrid that incorporates the best features of the linearization method with information from the underlying physical processes.

ACKNOWLEDGMENT

We wish to thank Paul Bryant of SBIR Inc. and Steve Solomon of Acumen Consulting for allowing us to use proprietary SBIR data within the present analysis. Without this assistance, the analysis could not have been progressed to the present level of understanding.

REFERENCES

1. R.G. Stockbridge, G.C. Goldsmith II, D.G. Edwards, A.G. Guertin, L.E. Jones and E.M. Olson, "Characterization and nonuniformity correction of a resistor array infrared scene projector," in *Characterization, Propagation, and Simulation of Sources and Backgrounds IV*, Proc. SPIE Vol. **2223**, 51-63 (1994).

2. L.E. Jones, E.M. Olson, R.L. Murrer Jr. and A.R. Andrews, "A simplified method for the hardware implementation of nonuniformity correction on a resistor array infrared scene projector," *in Technologies for Synthetic Environments: Hardware-in-the-loop Testing II*, Proc. SPIE Vol. 3084, 139-150 (1997).

3. E.M. Olson and R.L. Murrer Jr., "Non-uniformity correction of a resistor array infrared scene projector," in *Technologies for Synthetic Environments: Hardware-in-the-loop Testing IV*, Proc. SPIE Vol. 3697, 403-413 (1999).

4. B. Sieglinger, J. Norman, W.M. Meshell, D.S. Flynn, R.A. Thompson and G.C. Goldsmith II, "Array nonuniformity correction – new procedures designed for difficult measurement conditions," in *Technologies for Synthetic Environments: Hardware-in-the-loop Testing VIII*, Proc. SPIE Vol. 5092, 210-220 (2003).

5. C. Malone and D. Flynn, "Optimization of measurement process variables used in radiance uniformity calibration of the emitter source for the Wide Band Infrared Scene Projector (WISP)," in *Targets and Backgrounds: Characterization and Representation*, Proc. SPIE Vol. 2469, 118-131 (1995).

6. O.M. Williams, L.Świerkowski, R.A. Thompson, G.C. Goldsmith II and W.L. Herald, "Process-based real-time scene data processor design for emitter array infrared projectors," in *Technologies for Synthetic Environments: Hardware-in-the-loop Testing VII*, Proc. SPIE Vol. 4717, 120-135 (2002).

7. O.M. Williams, L.Świerkowski, A.J. Huber, J.D. Norman and G.C. Goldsmith II, "Infrared projector scene data real-time processor design," in *Technologies for Synthetic Environments: Hardware-in-the-loop Testing VIII*, Proc. SPIE Vol. 5092, 196-209 (2003).

8. G.C. Goldsmith II, W.L. Herald, R.A. Erickson, W.S. Irvine Jr., P.R. Mackin, P. Bryant and B. Lindberg, "Setting the PACE in IRSP: configurable PC-based array control electronic system for infrared scene projection," in *Technologies for Synthetic Environments: Hardware-in-the-loop Testing VIII*, Proc. SPIE Vol. 5092, 61-70 (2003).

9. E.M. Olson, O.M. Williams, R.L. Murrer Jr. and J.R. Kircher, "Resolution and dynamic range capabilities of dynamic infrared projection systems," in *Technologies for Synthetic Environments: Hardware-in-the-loop Testing V*, Proc. SPIE Vol. 4027, 202-213 (2000).

10. R.A. Joyce, L.Świerkowski and O.M. Williams, "infrared projector flood nonuniformity correction characteristics," in *Technologies for Synthetic Environments: Hardware-in-the-loop Testing VIII*, Proc. SPIE Vol. 5092, 185-195 (2003).

11. O.M. Williams, "Infrared photodetector background current estimation," Appl. Opt. 31, 497-503 (1992).

12. O.M. Williams, "Evaluation of emissive infrared projector radiant output parameters," in *Characterization, Propagation, and Simulation of Sources and Backgrounds II*, Proc. SPIE Vol. 1687, 402-414 (1992).

13. O.M. Williams, "Infrared projector effective blackbody temperature," Opt. Eng. 33, 230-236 (1994).

14. B. Cole, R. Higashi, J. Ridley, J. Holmen, R. Stockbridge, L. Murrer and E. Burroughs, "Large-area infrared microemitter arrays for dynamic infrared scene projection," in *Technologies for Synthetic Environments: Hardware-in-the-loop Testing III*, Proc. SPIE Vol. 3368, 57-70 (1998).

15. D.B. Beasley, D.A. Saylor and J. Buford, "BRITE II characterization and application to a new advanced flight motion simulator," in *Technologies for Synthetic Environments: Hardware-in-the-loop Testing VIII*, Proc. SPIE Vol. 5092, 24-34 (2003).

16. E.M. Olson and J.D. Potter, "Utilizing commercial-off-the-shelf PC graphics hardware for real-time hardware-in-the-loop scene generation," in *Technologies for Synthetic Environments: Hardware-in-the-loop Testing VIII*, Proc. SPIE Vol. 5092, 221-230 (2003).

17. P.V. Lyles, J.A. Buford Jr., D.S. Cosby and A.J. Mayhall, "Integration of COTS personal computers into a real-time hardware-in-the-loop for infrared image generation," in *Technologies for Synthetic Environments: Hardware-in-the-loop Testing VIII*, Proc. SPIE Vol. 5092, 231-239 (2003).

18. T.P. Bergin, "Application of innovative rendering techniques for hardware-in-the-loop (HIL) scene generation," in *Technologies for Synthetic Environments: Hardware-in-the-loop Testing VIII*, Proc. SPIE Vol. 5092, 240-246 (2003).

19. E.M. Olson, O.M. Williams and R.A. Thompson, "Optimization of resistor array infrared projector temporal response," in *Technologies for Synthetic Environments: Hardware-in-the-loop Testing VI*, Proc. SPIE Vol. 4366, 475-488 (2001).